

Journal Pre-proofs

A Gradient Reduction Strategy to Produce Defects-Rich Nano-Twin Cu Particles for Targeting Activation of Carbon-Carbon or Carbon-Oxygen in Furfural Conversion

Yanru Zhu, Jian Zhang, Xiaodan Ma, Zhe An, Shaowei Guo, Xin Shu, Hongyan Song, Xu Xiang, Jing He

PII: S0021-9517(20)30205-0
DOI: <https://doi.org/10.1016/j.jcat.2020.05.027>
Reference: YJCAT 13757

To appear in: *Journal of Catalysis*

Received Date: 21 March 2020
Revised Date: 13 May 2020
Accepted Date: 18 May 2020

Please cite this article as: Y. Zhu, J. Zhang, X. Ma, Z. An, S. Guo, X. Shu, H. Song, X. Xiang, J. He, A Gradient Reduction Strategy to Produce Defects-Rich Nano-Twin Cu Particles for Targeting Activation of Carbon-Carbon or Carbon-Oxygen in Furfural Conversion, *Journal of Catalysis* (2020), doi: <https://doi.org/10.1016/j.jcat.2020.05.027>

This is a PDF file of an article that has undergone enhancements after acceptance, such as the addition of a cover page and metadata, and formatting for readability, but it is not yet the definitive version of record. This version will undergo additional copyediting, typesetting and review before it is published in its final form, but we are providing this version to give early visibility of the article. Please note that, during the production process, errors may be discovered which could affect the content, and all legal disclaimers that apply to the journal pertain.

© 2020 Published by Elsevier Inc.



**A Gradient Reduction Strategy to Produce Defects-Rich Nano-Iwin Cu
Particles for Targeting Activation of Carbon-Carbon or Carbon-Oxygen in
Furfural Conversion**

*Yanru Zhu, Jian Zhang, Xiaodan Ma, Zhe An, Shaowei Guo, Xin Shu, Hongyan Song, Xu Xiang,
and Jing He**

State Key Laboratory of Chemical Resource Engineering& Beijing Advanced Innovation Center for
Soft Matter Science and Engineering, Beijing University of Chemical Technology, Beijing, China

*corresponding author. E-mail: jinghe@263.net.cn or hejing@mail.buct.edu.cn.

Postal address: Box 98, North Third Ring Road 15, Chaoyang District, Beijing, 100029, China

Abstract

Complexity of chemical linkages (C-C/C-H/C-O, C=C/C=O, or C-O-H/C-O-C) in biomass-derived molecules makes the selective activation of targeted bonds much more challenging, expecting well-defined catalysts and definite catalytically-active sites. This work demonstrates an effective gradient reduction strategy to control the definite structure of catalytically-active sites, affording defects-rich nano-twin Cu particles. This strategy just involves the reduction (calcination under H₂) of Cu^{II}-containing layered double hydroxides (LDHs) simply with controlling the reduction gradient (interval time) of Cu^{II} species in two chemical micro-environments (Cu^{II}-O-Cu^{II} and Cu^{II}-O-M^{II/III/IV} (M ≠ Cu)) in the brucite-like layer of LDHs. The nano-twin Cu particles efficiently promote the target activation of C-O and C=C in the conversion of furfural to cyclopentanone (CPO). With ~ 100 % furfural conversion, the defects-rich nano-twin Cu particles afford a CPO selectivity of 92 %, 50 % higher than regular spherical Cu particles. The multi-stepped defect sites, originating from the planar defects, play a decisive role in promoting the CPO selectivity by facilitating the hydro-deoxygenation to C-O of 4-hydroxycyclopentenone (HCP) and hydrogenation to C=C of HCP or cyclopentenone.

Keywords: gradient reduction strategy, nano-twin Cu particles, layered double hydroxides (LDHs), defects sites, furfural-to-cyclopentanone

1. Introduction

Cu is an earth-abundant and inexpensive 3d transition metal, and Cu or Cu-based nanoparticles perform well as catalyst in the selective activation of oxygen-containing chemical bonds, leading to hydrogenation, dehydrogenation, hydrogenolysis, or reforming of C-O and/or C=O under specific conditions [1-4]. Cu-based nanomaterials have thus been widely used in the catalytic conversion of biomass [5] and a variety of industrially promising or important reactions, including synthesis of alcohols from syngas [6] or CO₂ [7], steam reforming of methanol [8], oxidation of CO [9], water-gas shift reaction [10], selective hydrogenation of carbonyl compounds [11], and dehydrogenation of alcohols [12]. The conversion of oxygenates has been found to strongly depend on the structure of catalytically-active sites, and the activation of carbon-oxygen bonds is also structure-sensitive [13]. Grain boundaries (GBs), twin boundaries (TBs), and stacking faults are typical planar defects for metallic Cu, interrupting the periodicity of the atom arrangement and providing new possibilities in catalytic reactions with their unique electronic states [13]. Grain boundaries have been explored as high-active catalytic sites for CO₂ reduction [14] or CO reduction [15], which promotes the selectivity of CO or formic acid. Twin boundaries-rich Cu nanoparticles show enhanced selectivity in the electrochemical reduction of CO to C₂₊ products [16]. Atomic steps on the Cu surface, induced by planar defects and lattice strain of three-dimensionally ordered macroporous Cu-Fe catalysts, serve as high-activity oxygenation sites in the synthesis of higher alcohols from syngas [17]. Stepped Cu surface, created by the termination of a planar defect, is described as high energy sites for methanol synthesis over Cu/ZnO/Al₂O₃ industrial catalysts [7]. A dramatic increase in the activity and selectivity to H₂ and CO in the catalytic electroreduction of CO₂ has been observed by controlling the surface atomic coordination of model spherical Cu particles with decreasing Cu particle size [18]. Recently, artificially constructing defects on the surface of Cu particle to improve catalysis is growing more and more attractive [19]. GBs-rich Cu particles have been prepared by depositing Cu onto a film of aligned carbon nanotubes through e-beam evaporation [15]. Huang et al. reported fivefold twinned star decahedron Cu showing abundant surface defects at TBs terminations [20]. The twinned

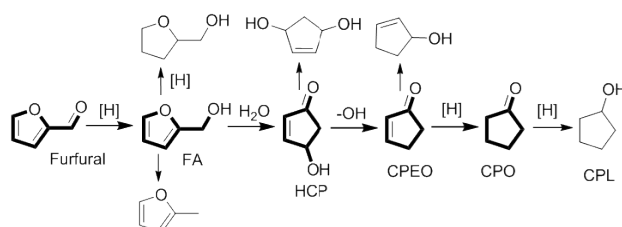
structure has been achieved by controlling the growth rate of Cu with weak reduction agent and low reduction temperature [20]. Three-dimensionally freestanding nano-twinned Cu structures, showing coherent twin boundaries, have been directly printed by a localized pulsed electro-deposition strategy [21]. High density of twin defects have been produced with Pt-Cu hierarchical quasi great dodecahedrons by directed growth of multiple branches on icosahedral seeds [22]. The fabrication of specific defect structures have made great achievements with bulk Cu nanoparticles. However, fine manipulation for the definite structures or surface defects of supported Cu nanoparticles remains as a grand challenge.

Here, this work reports a gradient reduction strategy to control the definite defect structure of supported Cu particles by producing nano-twin Cu particles from the topological transformation of Cu^{II}-containing layered double hydroxides (LDHs). LDHs, a well-known anionic clay, consists of positively charged brucite-like layer and exchangeable interlayer anions [23,24]. The brucite-like layer accommodates a wide range of divalent (M^{II}) and high-valence (M^{III} or M^{IV}) metal cations with the metal cations surrounded approximately octahedrally by hydroxide ions [23]. The octahedral units form infinite layers by edge-sharing [23], with M^{II}-O-M^{II} or M^{II}-O-M^{III/IV} linkage allowed while M^{III/IV}-O-M^{III/IV} linkage forbidden [25]. In virtue of the structural characteristics of brucite-like layer, LDHs have many potential applications in heterogeneous catalysis, functioning as catalyst, support, or catalyst precursor [26,27]. By calcination of reducible-metal containing LDHs under a H₂ atmosphere [28], supported metal nanoparticles can be produced, which is one of the significant applications of LDHs. Supported Cu has been produced from Cu-containing LDHs and the interfaces of Cu-support have been controlled [29]. Supported Ni has also been produced by the reduction of NiAl-LDHs [30,31], and interlayer anions (carbonate or nitrate) have been revealed to influence the exposure plane of Ni particles [30]. This work utilizes the difference in the chemical environments of divalent Cu cations (Cu^{II}-O-Cu^{II} and Cu^{II}-O-M^{III/IV} (M ≠ Cu)) to control the production of Cu⁰ from Cu^{II} in Cu^{II}-containing LDHs. By tailoring the temperature-programmed rate in the reduction of Cu^{II}-containing LDHs (Cu^{II}Zn^{II}Al^{III}Zr^{IV}-LDHs here), the reduction of Cu^{II}-O-Cu^{II} is segregated

kineutically from that of $\text{Cu}^{II}\text{-O-Zn}^{II}/\text{Cu}^{II}\text{-O-Al}^{III}/\text{Cu}^{II}\text{-O-Zr}^{IV}$, which is defined as gradient reduction in this work, and generates the defects-rich nano-twin Cu particles supported on Zn(Al)(Zr)O .

The catalytic conversion of biomass and biomass-derived platform molecules has attracted more and more attention for the urgent demand of sustainable and clean production of fuels and chemicals [32-34]. Amongst the platform molecules, furfural is one of the most promising compounds in sustainable production of value-added C_4/C_5 chemicals or derived biofuels [35]. However, just like other biomass-derived molecules, the chemical linkages (C-C/C-H/C-O, C=C/C=O, and C-O-H/C-O-C) in furfural are so diversified that the selective activation and directed conversion of targeted chemical bonds are of great challenge [36]. And that, the transformation of furfural to value-added or fine chemicals usually involve multiple successive steps [37], including hydrogenation of C=C and/or C=O [38,39], hydrogenolysis of C-O [40,41], hydro-deoxygenation [42], and/or rearrangement [43]. Each step could have competitive side-reactions, and even a change in the step sequence could lead to diverse products. Hydrogenation rearrangement of furfural to cyclopentanone (CPO) has been particularly attractive since it offers a clean and sustainable alternative to produce CPO [44], a very useful compound under heavy demand [45] but still relying exclusively on fossil-based feedstock [46,47]. According to previous report [48], the furfural-to-CPO reaction starts with the hydrogenation of C=O in furfural on metal sites, the resulting furfuryl alcohol (FA) is subsequently converted to 4-hydroxy-2-cyclopentenone (HCP) on acidic sites via a Piancatelli rearrangement, and finally the C-OH in HCP carries on selective hydro-deoxygenation followed by hydrogenation to C=C on metal sites to produce CPO. However, the process could be accompanied by side-reactions in each step (Scheme 1), such as hydrogenation to C=C in furfural or FA, C-OH breakage (hydrogenolysis) of FA, and hydrogenation to C=O in HCP or its derivative [35]. Conventional reforming and/or hydrogenation catalysts, widely applied in petrochemical industry, have once been applied to transform biomass-derived to fuels [49,50]. The development of well-defined catalysts [51,52] and definition of active sites [53] are supposed to help promoting the furfural-to-CPO transformation, as realized in other reactions of both model [53] and real [7] systems. Here, with the defects-rich nano-

twin Cu particles as catalyst, furfural has been efficiently converted to CPO in high selectivity. An effective breakage of C-O and targeted activation to C=C on well-defined defects-rich Cu particles are demonstrated.



Scheme 1. Proposed reaction pathway in hydrogenation of furfural.

2. Experimental

2.1. Materials

$\text{Cu}(\text{NO}_3)_2 \cdot 3\text{H}_2\text{O}$, $\text{Zn}(\text{NO}_3)_2 \cdot 6\text{H}_2\text{O}$, $\text{Al}(\text{NO}_3)_3 \cdot 9\text{H}_2\text{O}$, Na_2CO_3 , and NaOH were all of analytical purity and purchased from Sinopharm. $\text{ZrO}(\text{NO}_3)_2 \cdot 6\text{H}_2\text{O}$ (99.99%) was purchased from Aladdin. Furfuryl alcohol (98.0 %), cyclopentanone (99.0 %), cyclopentanol (99.0 %), and tetrahydrofurfuryl alcohol (97.0 %) were purchased from Alfa-Aesar. Furfural (99.0 %) was purchased from Acros Organics. 2-cyclopentenone (98.0 %), 1-hexanol (99.0 %), and 4-hydroxy-2-cyclopentenone (98.0 %) were purchased from Innochem. All chemicals were used as received without purification.

2.2. Preparation

The Cu, Zn, Al, Zr-containing layered double hydroxides (denoted as $\text{Cu}^{\text{II}}\text{Zn}^{\text{II}}\text{Al}^{\text{III}}\text{Zr}^{\text{IV}}$ -LDHs) with Cu/Zn/Al/Zr molar ratio of 2/7/2/1 ($M^{2+}/(M^{3+}+M^{4+}) = 3$, typical component of LDHs) was synthesized by a pH-constant co-precipitation method. Typically, $\text{Cu}(\text{NO}_3)_2 \cdot 3\text{H}_2\text{O}$ (12 mmol), $\text{Zn}(\text{NO}_3)_2 \cdot 6\text{H}_2\text{O}$ (42 mmol), $\text{Al}(\text{NO}_3)_3 \cdot 9\text{H}_2\text{O}$ (12 mmol), and $\text{ZrO}(\text{NO}_3)_2 \cdot 6\text{H}_2\text{O}$ (6 mmol) were dissolved together in 200 mL of deionized water, which was referred to as solution A. Solution B was a mixture of NaOH (120 mmol) and Na_2CO_3 (31.5 mmol) ($[\text{OH}^-] = 1.6[\text{M}^{2+} + \text{M}^{3+} + \text{M}^{4+}]$ and $[\text{CO}_3^{2-}] = 2[\text{M}^{3+} + \text{M}^{4+}]$) in 200 mL of deionized water. Solution A and B were simultaneously added dropwise to a four-necked flask containing 200 mL of deionized water under constant pH (9.0). After

aging at 65 °C for 12 h, the solid was nitrated, washed thoroughly with deionized water till the nitrate is neutral, and dried at 80 °C overnight, to give Cu^{II}Zn^{II}Al^{III}Zr^{IV}-LDHs. Similar procedure was used to prepare Zn^{II}Al^{III}Zr^{IV}-LDHs (Zn/Al/Zr molar ratio of 9/2/1) sample in the absence of Cu(NO₃)₂·3H₂O. Cu^{II}Zn^{II}Al^{III}Zr^{IV}-LDHs was reduced under H₂ atmosphere at 450 °C (to insure the LDHs completely turn into layered double oxide (Zn(Al)(Zr)O) supported Cu) for 2 h in a tube-furnace with the temperature programmed from ambient to 450 °C in 2 °C min⁻¹. After the tube-furnace was cooled to ambient, 10 % H₂/N₂ was introduced into the furnace for 2 h. The reduced sample, denoted Cu⁰-Zn(Al)(Zr)O-2, was used for catalytic reaction and characterization immediately. Cu^{II}Zn^{II}Al^{III}Zr^{IV}-LDHs was reduced under H₂ atmosphere at 450 °C for 2 h in a tube-furnace with the temperature programmed from ambient to 450 °C in 10 °C min⁻¹. After the tube-furnace was cooled to ambient, 10 % H₂/N₂ was introduced into the furnace for 2 h. The reduced sample, denoted Cu⁰-Zn(Al)(Zr)O-10, was used for catalytic reaction and characterization immediately. ZnAlZr-LDHs was calcinated at 450 °C for 2 h under H₂ atmosphere with the temperature programmed from ambient to 450 °C in 2 °C min⁻¹, to give Zn(Al)(Zr)O.

2.3. Characterizations

Quantification of Cu was performed using a Shimadzu ICPS-75000 inductively coupled plasma optical emission spectrometer (ICP-OES). Before the measurements, 30 mg of sample was dissolved in 5 mL of nitric acid at ambient. The solution was transferred to a 10-mL volumetric flask, and diluted with deionized water to volume. Powder X-ray diffraction (XRD) patterns were recorded with a Shimadzu XRD-6000 diffractometer (Cu K α radiation, $\lambda = 0.154$ nm) in the 2θ ranges of 3–80 ° with a scan speed of 5 ° min⁻¹. Transmission electron microscope (TEM) images were taken with JEOL 2100 high resolution transmission electron microscope operating at an accelerating voltage of 200 kV. The sample for TEM measurements was dispersed in ethanol under ultrasonic conditions before depositing on Cu micro grids, and covered by a carbon coating of several nanometers to prevent from charging the sample. The size distribution of Cu was based on at least 300 particles in total counted in varied regions. High-angle annular dark-field scanning (HAADF-STEM) images

were taken on a JEM-ARM 200F electron microscope capable of sub-angstrom resolution. H₂-temperature programmed reduction (H₂-TPR) was carried out on a Micrometric ChemiSorb 2750 chemisorption system with a thermal conductivity detector (TCD). About 100 mg of sample was loaded in a U type quartz reactor. The TPR was carried out with a heating ramp rate of 2 °C min⁻¹ or 10 °C min⁻¹ in a stream of 10 % H₂ in Ar from 50 °C to 600 °C, with a total flow rate of 40 mL min⁻¹. The samples were dispersed onto a Au grid coated with a thin holey carbon film. The dispersion of Cu was determined by N₂O oxidation followed by H₂ titration using the procedure described by previously reports [54,55]. Typically, about 50 mg of reduced Cu-containing sample was loaded in a U-type quartz reactor and pre-treated online at 350 °C for 1 h under 10 % H₂/Ar mixture (40 mL min⁻¹). Afterward, the sample was cooled to 70 °C in a flow of Ar (40 mL min⁻¹). Then pulse N₂O was introduced into the carrier gas until N₂O peak reached saturation to completely oxidize the surface metallic Cu. The sample was then cooled to room temperature and followed by a H₂-TPR. H₂-TPR was carried out with a heating ramp rate of 10 °C min⁻¹ in 10 % H₂/Ar mixture to 400 °C, with a total flow rate of 40 mL min⁻¹. The amount of consumed H₂ was recorded by TCD. It was assumed that one hydrogen molecule reduced one surface Cu₂O to Cu. The Cu dispersion is defined as the fraction of Cu atoms exposed at the surface, and was calculated as follows:

$$D_{\text{Cu}} = \frac{N_{\text{surface}}}{N_{\text{total}}} = \frac{\text{amount of consumed H}_2}{N_{\text{total}} \text{ (by ICP)}} \times 100\%$$

Quasi-in-situ X-ray photoelectron spectra (XPS) were recorded on a Thermo Fisher Scientific ESCALAB-250 instrument (USA) with an excitation source of Al Ka radiation. A C1s peak at 284.8 eV was used as a calibration peak. In addition to a binding energy scan range from 0 to 1200 eV for the identification of all detectable elements, detailed scans for chemical state identification and quantification were recorded. Quasi-in-situ Cu K-edge X-ray absorption spectra (XAS) were recorded on the 1W1B beamline of the Beijing Synchrotron Radiation Facility (BSRF) operated at 2.2 GeV and 200 mA. A Si (111) double-crystal monochromator was used to reduce the harmonic component of the monochrome beam. All the samples were measured in the transmission mode. Before measurements, the as-prepared Cu-containing sample was pretreated carefully to ensure that the

reduced sample was not exposed to air. Specimens were made by directly applying the fine powders to Scotch tape inside a glove box kept under vacuum package, sealed by the valve bag. The IFEFFIT software was used to analyze the extended X-ray fine structure (EXAFS) data at the Cu K-edge. For temperature-programmed desorption of ammonia (NH₃-TPD) test, about 100 mg of reduced sample was first activate at 400 °C for 1 h in 10 % H₂/Ar, followed by purging with high purity Ar (50 mL min⁻¹) for 1 h at 410 °C. Afterward, as the temperature decreased to 50 °C, NH₃ was injected until saturation. NH₃-TPD was carried out with a heating ramp rate of 10 °C min⁻¹ to a sample temperature of 500 °C. The calibration curve for the NH₃ amount as a function of the peak area was done in advance and the amount of acid sites was calculated according to the area of desorption peaks. In situ Fourier transform infrared (FT-IR) spectra for CO or CPEO adsorption, and in situ FT-IR spectra for the hydrogenation of HCP were recorded on Nicolet 380 model (Thermo Electron Corporation) equipped with an MCT-A detector cooled by liquid nitrogen. KBr beam-splitter was used to obtain spectra in the range of 4000-650 cm⁻¹. The spectrum was collected at a spectrum resolution of 2 cm⁻¹ and an accumulation of 64 scans. About 15 mg of the sample was pressed into a disk for each experiment. Before measurements, the reduced sample was pretreated in situ by a flowing of H₂ (20 mL min⁻¹) at 400 °C for 1 h. For IR measurement of CO adsorption, the reduced sample was cooled down to 30 °C in Ar. Then the sample was exposed to CO flow (20 mL min⁻¹) at 30 °C for 1 h followed by purging with Ar to remove gaseous CO for 15 min. The FTIR spectra were recorded. The resulting spectra have deducted the background at 30 °C. For IR measurement of CPEO adsorption, the reduced sample was cooled down to 50 °C in Ar. Then, pure CPEO was introduced by flowing Ar for 30 min at 50 °C. The FT-IR spectra were recorded intervals of Ar flushing. The resulting spectra have deducted the absorption of gaseous CPEO and the background. For IR measurement of HCP hydrogenation, the reduced sample was cooled down to 100 °C in Ar. Then, pure CPEO was introduced by vacuum depression vaporization, and purged in Ar to remove the gaseous and weakly adsorbed HCP for 30 min. With the introducing of H₂ flow (20 mL min⁻¹), the spectra of the hydrogenation reaction process were recorded intervals of H₂ flow at 100 °C. The resulting spectra

have deducted the absorption of gaseous H₂O and the background. ¹H and ¹³C nuclear magnetic resonance (NMR) spectra were recorded on a Bruker AV-400 (400 MHz) spectrometer. Chemical shifts were reported in parts per million (ppm). High resolution mass spectra (HRMS) were obtained on a XEVO-G2QTOF spectrometer and were reported as m/z (relative intensity).

2.4. Catalytic tests

General procedure for the liquid phase hydrogenation conversion of furfural in a autoclave reactor: Typically, furfural (5.2 mmol, 0.5 g), catalyst (25 mg) and ultrapure water (10 mL) were placed into a stainless-steel autoclave reactor with a magnetic stirrer, and then the reactor was sealed and flushed with pure hydrogen for four times. Subsequently, the reactor was charged with pure hydrogen to 2.5 MPa. After that, the reactor was heated to 160 °C, and the pressure was increased to 4.0 MPa. The reaction was initiated by stirring at a speed of 800 rpm. During the reaction, the hydrogen pressure was kept constant by supplying hydrogen continuously from gas cylinder through the pressure regulator to compensate for the consumed hydrogen in the reactor. After the reaction, the reactor was rapidly cooled to room temperature and then depressurized. The organic products were extracted by dichloromethane from the liquid and then analyzed by gas chromatograph (Shimadzu GC-2014C) equipped with a inno-WAX capillary column (30.0 m × 250 μm × 0.25 μm). The product was purified via silica column chromatography (eluted with ethyl acetate and acetonitrile) for NMR and MS measurements. The amounts of products were determined based on GC data using the internal standard method (*n*-hexanol as the internal standard). The conversion of furfural (%) and the selectivity of main products (%) were calculated by

$$\text{Conversion} = \left(1 - \frac{\text{mol of furfural}}{\text{mol of furfural loaded initially}}\right) \times 100\% \quad \text{and}$$

$$\text{Selectivity of product} = \frac{\text{mol of product}}{\text{mol of furfural converted}} \times 100\%$$

Procedure for the conversion of furfural in a continuous-flow reactor: The conversion of furfural to CPO was also carried out in a vertical fixed-bed reactor. The catalyst was pelletized and sieved to 20–40 mesh size. Then, 0.5 g of the reduced sample was loaded in a stainless steel tubular reactor

with an inner diameter of 10 mm and a length of 500 mm. The reaction was operated at 160 °C and 2 MPa H₂, with a H₂ flow of 50 mL min⁻¹. The feedstock comprising a diluted aqueous solution of furfural (5 wt%) was continuously introduced into the reactor by an HPLC pump. The products were obtained when the reaction reached the steady state. The liquid and gas products were cooled and collected in a gas-liquid separator immersed in an ice-water trap. The liquid products were analyzed by the same procedures as the liquid phase hydrogenation conversion in a autoclave reactor above.

3. Results and discussion

3.1. Nano-twin Cu particles produced by gradient reduction strategy

In this work, Zn, Al, and Zr-containing mixed metal oxides (Zn(Al)(Zr)O) supported Cu particles was produced from Cu^{II}Zn^{II}Al^{III}Zr^{IV}-LDHs. Cu^{II}Zn^{II}Al^{III}-LDHs is a classical precursor [56] for producing Zn(Al)O supported Cu, and Zr^{IV}-doping is to provide suitable acidity [57] in the catalytic reaction. In the X-ray diffraction (XRD) pattern of Cu^{II}Zn^{II}Al^{III}Zr^{IV}-LDHs (Fig. S1), the (003), (006), (009), (015), (018), (110), and (113) reflections typical of hydrotalcite structure are clearly observed at $2\theta = 11.8, 23.5, 34.6, 39.1, 46.6, 60.1, \text{ and } 61.3^\circ$. No other crystallite phases are resolved. Then Cu^{II}Zn^{II}Al^{III}Zr^{IV}-LDHs was reduced with H₂ under 450 °C. In the reduction, the temperature was programmed from room temperature to 450 °C in 2 °C min⁻¹, affording Cu⁰-Zn(Al)(Zr)O-2. The Cu content was determined to be 11.2 wt% and the specific surface area was 86.5 m²/g for Cu⁰-Zn(Al)(Zr)O-2 (Table S1). In the XRD pattern of Cu⁰-Zn(Al)(Zr)O-2, the reflections characteristic of Cu⁰ or ZnO are clearly observed, while no reflections of LDHs exists (Fig. S1). The observations indicate Cu^{II}Zn^{II}Al^{III}-LDHs has been completely transformed to mixed metal oxides supported Cu⁰ species (Cu⁰-Zn(Al)(Zr)O-2) in the thermal treatment and reduction with H₂. According to TEM image (Fig. 1a), Cu particles in Cu⁰-Zn(Al)(Zr)O-2 are well-dispersed on the surface of Zn(Al)(Zr)O with a maximum size distribution of around 4.6 nm. The Cu dispersion was 17.7 % for Cu⁰-Zn(Al)(Zr)O-2. In the high-angle annular dark-field scanning transmission electron microscopic (HAADF-STEM) images, each Cu particle for Cu⁰-Zn(Al)(Zr)O-2 is irregular and

consists of at least two partially overlapped Cu ensembles, exhibiting a visible nano-twinned structure (Fig. 1b and 1c). Focusing on one Cu nano-twin particle, diversified planar defects are observed, including dislocations, stacking faults, and twin boundaries (Fig. 1d). The planar defects result in surface kinks (green lines) at the termination of twin boundaries (Fig. 1e), constituting multi-stepped surface defects. Visible ZnO species, showing 100 plane, are observed surrounding the Cu nano-twin particles (Fig. S2), and the presence of disordered $\text{Cu}^0\text{-ZnO}_x$ interfaces are also observed. The growth orientation of 111 plane for Cu nano-twin particle exactly matches the growth orientation for ZnO species, indicative of the induction or promotion of ZnO (100) to Cu nano-twin particles. No CuZn alloy has been resolved. The role of ZnO on nano-twinned structure of Cu particles deserves an in-depth research that is under investigation in our laboratory. For comparison, $\text{Cu}^0\text{-Zn(Al)(Zr)O-10}$ was prepared by calcination of $\text{Cu}^{\text{II}}\text{Zn}^{\text{II}}\text{Al}^{\text{III}}\text{Zr}^{\text{IV}}\text{-LDHs}$ in H_2 under 450 °C with the temperature programmed rate raised to 10 °C min^{-1} . $\text{Cu}^0\text{-Zn(Al)(Zr)O-10}$ possesses a specific surface area of 88.7 m^2/g , a Cu dispersion of 18.4 % (Table S1), and a Cu particle size of around 4.6 nm (Fig. S3), all similar to $\text{Cu}^0\text{-Zn(Al)(Zr)O-2}$. While in the HAADF-STEM image of $\text{Cu}^0\text{-Zn(Al)(Zr)O-10}$ (Fig. S4), only regular surface defects are observed, resulting from the regular spherical fcc particles or Wulff polyhedra. However, based on the STEM images only, it is hard to distinguish whether the observed moire patterns are defects in nano-twin or the projections from the overlapped individual crystals. More convinced investigations will be carried out in the following sections.

Extended X-ray absorption fine structure (EXAFS) spectra, CO adsorbed Fourier-transformed infrared (FT-IR) spectra, and XPS spectra were applied to further reveal the local coordination environment, surface defects, and chemical states of nano-twin Cu particles. According to EXAFS results (Fig. 1f and Table S2), the Cu-Cu coordination number (7.8) for $\text{Cu}^0\text{-Zn(Al)(Zr)O-2}$ is lower than that for $\text{Cu}^0\text{-Zn(Al)(Zr)O-10}$ (8.5), and the Cu-Cu Debye-Waller factor (0.011) for $\text{Cu}^0\text{-Zn(Al)(Zr)O-2}$ is higher than that for $\text{Cu}^0\text{-Zn(Al)(Zr)O-10}$ (0.009), suggesting a more severely distorted Cu environment associated with abundant Cu defects for nano-twin Cu particles. In the FT-IR spectra with CO adsorbed (Fig. 1g), both $\text{Cu}^0\text{-Zn(Al)(Zr)O-2}$ and $\text{Cu}^0\text{-Zn(Al)(Zr)O-10}$ present the

bands at 2106 and 2093 cm^{-1} , which can be assigned [58] to the CO adsorption on Cu defect sites (such as step or edge sites) and Cu terrace sites of low index planes. According to the relative area of absorption bands, Cu defect sites are estimated to account for 56 % for $\text{Cu}^0\text{-Zn(Al)(Zr)O-2}$, and only 21 % for $\text{Cu}^0\text{-Zn(Al)(Zr)O-10}$. The nano-twinned Cu particles in $\text{Cu}^0\text{-Zn(Al)(Zr)O-2}$ provide more surface defect sites than regular spherical nanoparticles in $\text{Cu}^0\text{-Zn(Al)(Zr)O-10}$, which supports the observations in STEM images. In quasi-in situ Cu $2p_{3/2}$ XPS spectra (Fig. 1h and 1i), the binding energy around 932 eV, corresponding to the Cu^0 and/or Cu^I state, [59] is observed for both $\text{Cu}^0\text{-Zn(Al)(Zr)O-2}$ and $\text{Cu}^0\text{-Zn(Al)(Zr)O-10}$. But in the Cu LMM X-ray excited Auger electron spectra (XAES), only the kinetic energy at 918.9 eV, corresponding to the Cu^0 state [60] is observed. So it is approved that Cu is mainly present in metallic state for both $\text{Cu}^0\text{-Zn(Al)(Zr)O-2}$ and $\text{Cu}^0\text{-Zn(Al)(Zr)O-10}$.

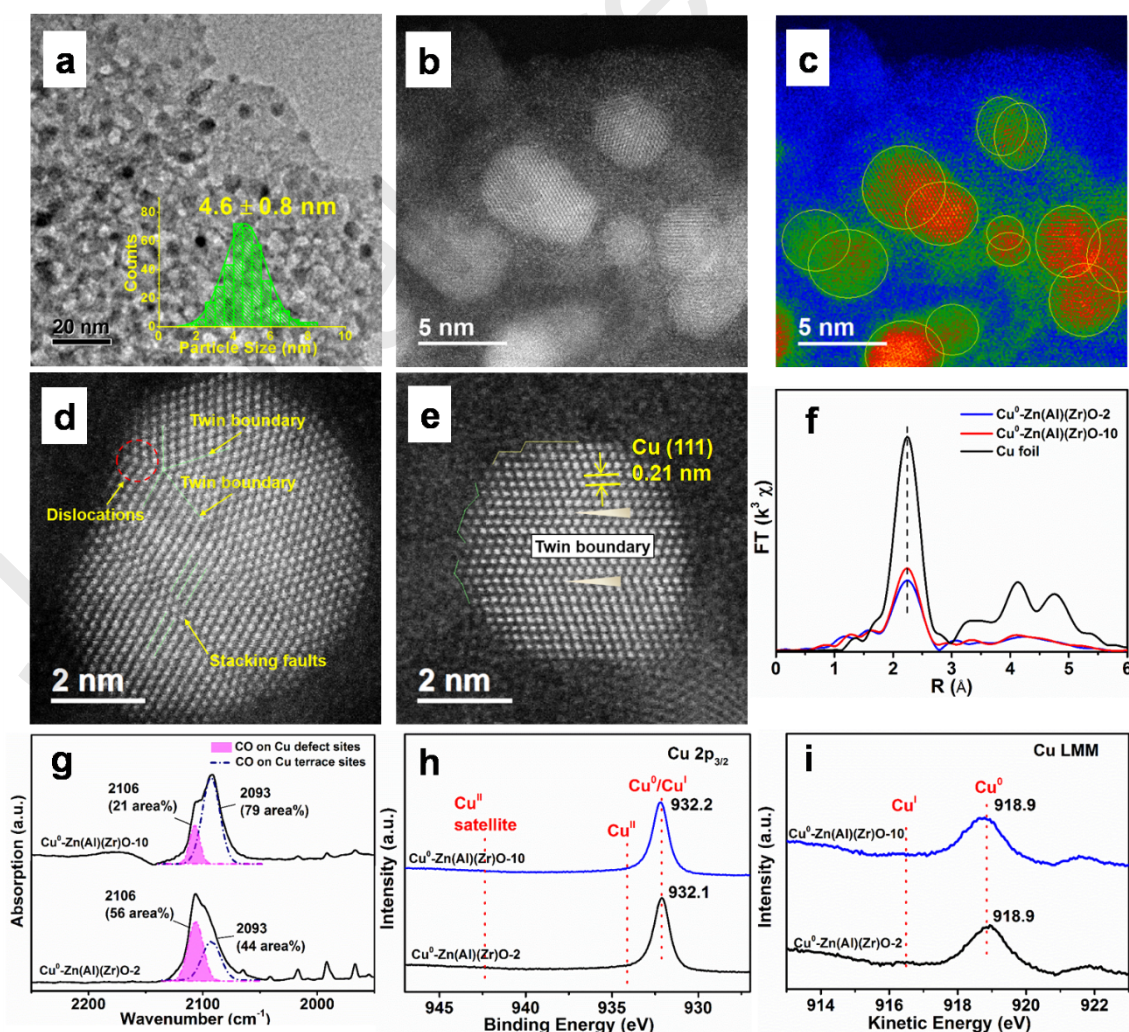


Fig. 1. (a) TEM image of Cu⁰-Zn(Al)(Zr)O-2 with particle size distribution (inset); (b-e) HAADF-STEM images for Cu nano-twin particles in Cu⁰-Zn(Al)(Zr)O-2 with coloured intensity map (c), displaying polytype planar defects (d) and highlighted stepped surfaces (e); (f) Fourier-transform of the k³-weighted EXAFS spectra at the Cu K-edge; (g) FT-IR spectra for CO adsorbed at 303 K followed by Ar purge for 15 min; (h) Cu 2p_{3/2} XPS, and (i) Cu LMM XAES spectra.

As discussed above, the two designed temperature-programmed rates during the reduction are the key factors for the distinctive structures. To reveal the origin of nano-twin Cu particles, H₂-TPR measurements of Cu^{II}Zn^{II}Al^{III}Zr^{IV}-LDHs were performed with a temperature-programmed rate of 2 or 10 °C min⁻¹. Besides, the reduction of ZnAlZr-LDHs (without Cu) to produce Zn(Al)(Zr)O was introduced as a control. As observed in Fig. S5, no visible H₂ consumptions is observed for ZnAlZr-LDHs in the range of 100-400 °C. For the reduction of Cu^{II}Zn^{II}Al^{III}Zr^{IV}-LDHs, two H₂ consumptions are observed in either case, which can be attributed to the reduction of Cu^{II}-O-Cu^{II} and Cu^{II}-O-M (here M = Zn, Al, or Zr) species in Cu^{II}Zn^{II}Al^{III}Zr^{IV}-LDHs, according to the previous report [61]. No big differences have been revealed except that the reduction temperature of either Cu^{II}-O-Cu^{II} or Cu^{II}-O-M species with a heating rate of 2 °C min⁻¹ is about 20 °C lower than that with a heating rate of 10 °C min⁻¹. The reduction kinetics changes with varied temperature-programmed rate, and the integral areas from the reduction of Cu^{II} are incomparable, while the amounts of H₂ consumption should be constant. So the H₂-TPR profiles have been transformed to H₂ consumption as a function of time (Fig. 2a). Theoretically, the integral area for heating rate of 2 °C min⁻¹ is similar to that for heating rate of 10 °C min⁻¹ in the H₂-TPR profiles. Interestingly, the time interval between the reduction of Cu^{II}-O-Cu^{II} and Cu^{II}-O-M species is about 40 min for a heating rate of 2 °C min⁻¹, while only 6 min for 10 °C min⁻¹. That is, in a slower temperature-programmed rate (2 °C min⁻¹ here), after Cu^{II}-O-Cu^{II} species has gone through the conversion to Cu⁰ and a formation of primary Cu ensembles for about 40 min, Cu^{II}-O-M species has just started to be reduced. So the Cu⁰ species from Cu^{II}-O-M has the chance to grow onto the primary Cu ensembles already from Cu^{II}-O-Cu^{II} but with another growth orientation,

thus affording nano-twin Cu particles. We call such a reduction process as gradient reduction. The gradient reduction of Cu^{II} and the formation of nano-twin Cu particles have been directly visualized from in situ HR-TEM images (Fig. 2b-f). In the in situ calcination of $\text{Cu}^{\text{II}}\text{Zn}^{\text{II}}\text{Al}^{\text{III}}\text{Zr}^{\text{IV}}$ -LDHs under H_2 from ambient temperature in $2\text{ }^\circ\text{C min}^{-1}$, irregular clusters are observed to emerge at $150\text{ }^\circ\text{C}$ (Fig. 2b). With temperature held at $150\text{ }^\circ\text{C}$, the cluster gradually grows, affording an ensemble (1) with size of $\sim 3\text{ nm}$ and an interplanar spacing of 0.209 nm attributed to Cu (111) (Fig. 2c and 2d). In about 150 s, another ensemble (2) appears and grows at upper right of Cu ensemble (1) (Fig. 2e), and finally forming a nano-twined Cu particle with two partially overlapped Cu ensembles (Fig. 2f). The in situ HR-TEM results provide strong evidence for the origin of nano-twin Cu particles by a reduction of $\text{Cu}^{\text{II}}\text{-O-M}$ specie after the reduction of $\text{Cu}^{\text{II}}\text{-O-Cu}^{\text{II}}$ specie, rather than the aggregation of two individual Cu particles. So defects-rich nano-twin Cu particles could be conveniently prepared from Cu-containing LDHs by a gradient reduction process of Cu^{II} in different chemical micro-environments. This gradient reduction strategy, originally proposed here, could also be extended to developing diverse defects-rich supported nano-metallic materials. However, due to the existence of the energy from the electron beam in TEM, the reduction of $\text{Cu}^{\text{II}}\text{Zn}^{\text{II}}\text{Al}^{\text{III}}\text{Zr}^{\text{IV}}$ -LDHs occurs in a lower temperature under the conditions of in situ TEM experiment than that under practical condition. The evidence from in situ TEM experiment could not powerfully explain the difference in reduction behavior between two heating rates (2 and $10\text{ }^\circ\text{C min}^{-1}$). This deserves an in-depth investigation using more suitable in situ characterization techniques, and further study is being carried out in our laboratory.

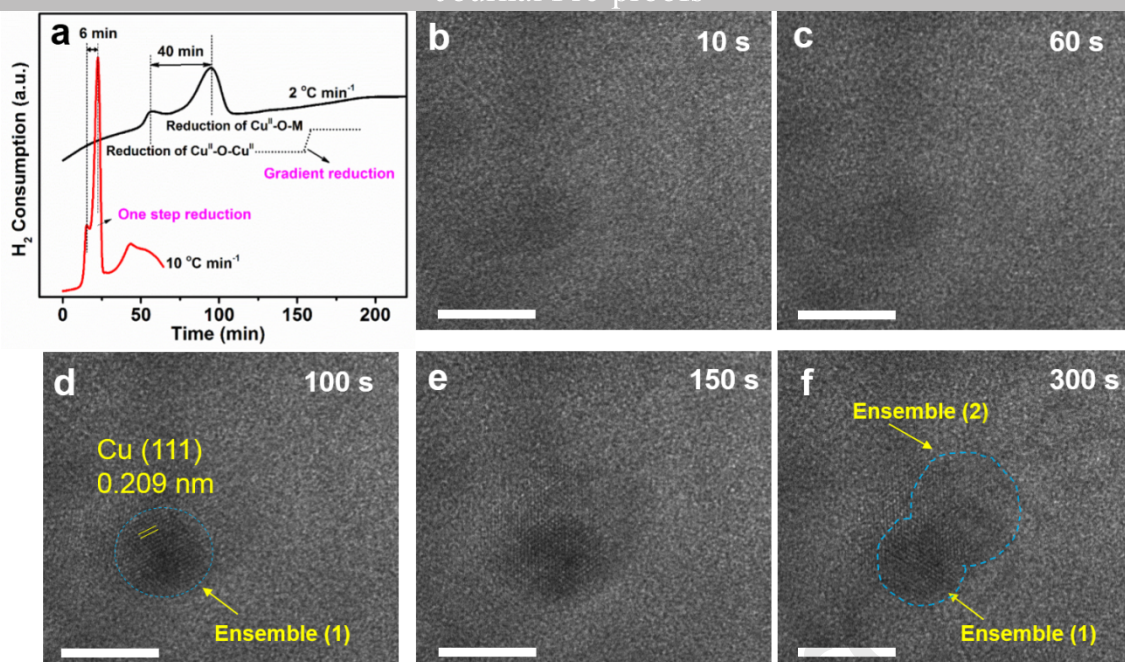


Figure 2. (a) H₂-TPR profiles as a function of time for Cu^{II}Zn^{II}Al^{III}Zr^{IV}-LDHs with a temperature programmed rate of 2 or 10 °C min⁻¹. Sequential HR-TEM images (b-f) from the same area in the in situ calcination of Cu^{II}Zn^{II}Al^{III}Zr^{IV}-LDHs under H₂ at 150 °C. A 5 nm scale bar in b-f.

3.2. Catalytic performance of defects-rich nano-twin Cu particles

The Zn(Al)(Zr)O supported Cu particles were applied as the catalysts for the aqueous phase hydrogenation of furfural in autoclave reactor under 2.5 MPa initial H₂ pressure and 160 °C. The qualitative identification of each product are based on the results from ¹H and ¹³C nuclear magnetic resonance (NMR) spectra and mass spectra (MS) (see details in the Supporting Information, Appendix). Regular Cu particles (Fig. 3a left) exhibit more sluggish kinetics of furfural-to-CPO conversion than nano-twin Cu particles (Fig. 3b left). FA, HCP, and CPEO as intermediates are detected in either case. Over regular spherical Cu particle, a CPO selectivity of 61.5 % with furfural conversion of 96.0 % in 3 h has been achieved, with the selectivity to HCP and CPEO of up to 11.5 % and 20.1 %. With the reaction time prolonged to 4 h, neither HCP nor CPEO is transformed completely, and meanwhile the over-hydrogenation of C=O in CPO (to CPL) is observed visibly. Over defects-rich nano-twin Cu particles, a selectivity of 92.3 % to CPO with an almost complete conversion of furfural in 3 h has been afforded (Fig. 3b). With the reaction time prolonged to 4 h,

both HCP and CPEO have been transformed completely. The results indicate the defect sites on the surface of nano-twin particles are highly efficient for the selective hydro-deoxygenation of C-OH in HCP and the selective hydrogenation to C=C in CPEO.

The catalytic conversion of HCP (Fig. 3, right), one of the major intermediates in the conversion of furfural to CPO, confirms the superior catalysis of nano-twin Cu particles to that of regular spherical Cu particles. In the selective hydro-deoxygenation of HCP, nano-twin Cu particles afford a complete conversion of furfural within 90 min. The conversion of CPEO is accomplished in 2.5 h, and the yield of CPO approaches 100 %. No visible excessive hydrogenation product (CPL) has been detected. On regular spherical Cu particles, however, neither HCP nor CPEO has been complete transformed in 2.5 h, while excessive hydrogenation from CPO to CPL is clearly observed.

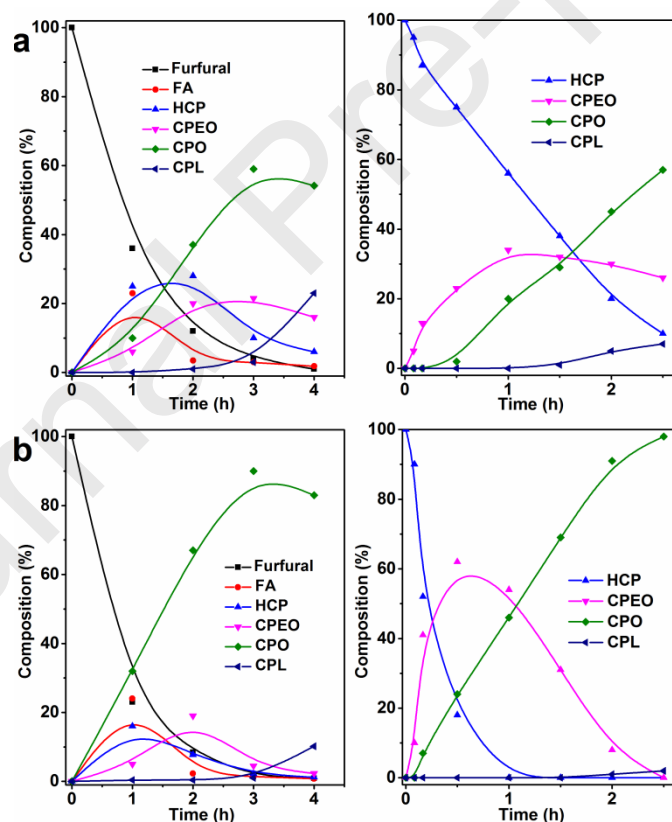


Fig. 3. Reaction progress profiles of liquid phase hydrogenation under 2.5 MPa initial H_2 pressure of furfural at 160 °C (left) and HCP at 100 °C (right) over (a) regular spherical Cu particle in in Cu^0 -Zn(Al)(Zr)O-10 and (b) nano-twin Cu particle in in Cu^0 -Zn(Al)(Zr)O-2.

To further confirm the structure-function relationship discovered above, the as-prepared $\text{Cu}^0\text{-Zn(Al)(Zr)O-2}$ was re-treated by calcination in N_2 at $450\text{ }^\circ\text{C}$ for 2 h followed by holding in H_2 at $450\text{ }^\circ\text{C}$ for 2 h (denoted $\text{Cu}^0\text{-Zn(Al)(Zr)O-2-R}$). The defects-rich Cu nano-twin particles in $\text{Cu}^0\text{-Zn(Al)(Zr)O-2}$ are transformed to regular spherical Cu particles in $\text{Cu}^0\text{-Zn(Al)(Zr)O-2-R}$ (Fig. S6). Based on the FT-IR results of CO adsorption, the percentage of Cu defect sites for $\text{Cu}^0\text{-Zn(Al)(Zr)O-2-R}$ has been decreased to 31 %, just at a similar level to that for $\text{Cu}^0\text{-Zn(Al)(Zr)O-10}$ (Fig. S7). By testing the intrinsic catalysis in a continuous-flow system, $\text{Cu}^0\text{-Zn(Al)(Zr)O-2}$ affords a CPO formation rate of $77\text{ mmol/mol}_{(\text{surface Cu})}/\text{s}$, while only $40\text{ mmol/mol}_{(\text{surface Cu})}/\text{s}$ for $\text{Cu}^0\text{-Zn(Al)(Zr)O-2-R}$ and $24\text{ mmol/mol}_{(\text{surface Cu})}/\text{s}$ for $\text{Cu}^0\text{-Zn(Al)(Zr)O-10}$ in same case (Fig. 4). With the decrease in Cu defect sites, CPO formation rate accordingly decreases. It is clear that surface Cu defects is one important factor to efficiently promote the selectivity of CPO.

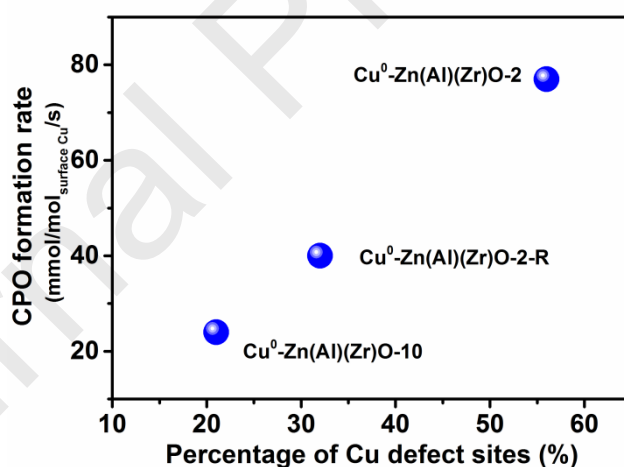


Fig. 4. (a) Variation of CPO formation rate with the percentage of Cu defect sites at < 20% furfural conversion, under 2 MPa H_2 pressure at $160\text{ }^\circ\text{C}$ in a fixed-bed reactor.

The in situ FT-IR spectra for HCP hydrogenation were further recorded (Fig. 5) to elucidate the role of surface defects of nano-twin Cu particles in the selective hydrogenation of C-OH, C=O, and C=C bonds. The absorption bands assigned to C=O at 1710 and 1672 cm^{-1} , C=C at 1584 cm^{-1} on

defects-rich nano-twin Cu particles and 1579 cm^{-1} on regular spherical Cu particles, C=C at 1194 cm^{-1} , C-O adsorbed with O terminal in linear at 1107 cm^{-1} , and C-O adsorbed with O terminal in bridged mode at 1052 cm^{-1} are observed. On defects-rich Cu particles, the bands assigned to C-O in O-terminal adsorption gradually decrease in intensity and eventually disappear with on-stream time under hydrogenation conditions, indicative of an efficient cleavage of C-O linkage, which is not visibly observed on regular spherical Cu particles. On defects-rich Cu particles, a new band at 1273 cm^{-1} , assigned to η^2 -type adsorbed C-O [62,63], emerges and gradually increases in intensity with the vanishment of O-terminal adsorption. This transformation of adsorbed C-O (from O-terminal adsorption to simultaneous adsorption of C and O) benefits the breakage of C-O, well accounting for more efficient hydro-deoxygenation to C-O in HCP on defects-rich Cu than on regular spherical Cu. The C=C absorption decreases rapidly in intensity till disappears whilst leaving the C=O unchanged on defects-rich Cu particles. Visible weakening of both C=O and C=C absorption, whilst none disappearing, has been observed on regular spherical Cu particles. This illuminates a highly selective hydrogenation to C=C, rather than to C=O, on defects-rich Cu surface. To clarify the activation to C=C in HCP or CPEO, the FT-IR spectra with CPEO adsorbed are recorded. Since no FT-IR spectra of CPEO adsorption has been reported previously, the FT-IR spectrum of CPEO in gaseous state has first been recorded (Fig. S8). Adsorbed on defects-rich Cu surface, the absorption band of C=C is observed at same position as that in gaseous state (Fig. 5a). With Ar purging, the intensity of $\nu(\text{C}=\text{C})$ fleetly decreases in intensity and eventually disappears on defects-rich Cu, indicative of the activation of C=C and subsequent conversion to C-C (Fig. 5a). But such adsorption and activation to C=C in CPEO are not observed on regular spherical Cu particles (Fig. 5b). The FT-IR results therefore suggest that the distinctive defects on nano-twin Cu surface play a decisive role in promoting the CPO selectivity by facilitating the selective hydro-deoxygenation of C-O in HCP and selective hydrogenation to C=C in HCP and CPEO.

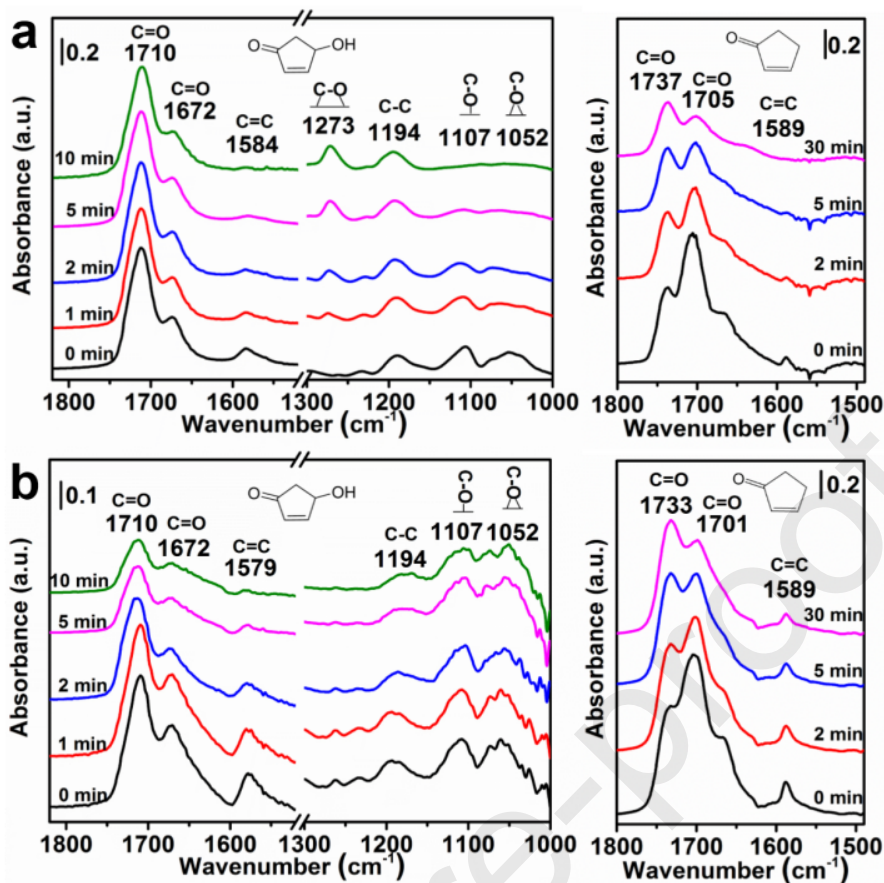


Fig. 5. Operando FT-IR spectra of HCP hydrogenation process (left) at 100 °C recorded at intervals of H₂ flow (0, 1, 2, 5, and 10 min), and FT-IR spectra of CPEO adsorption (right) at 50 °C recorded at intervals of Ar flushing (0, 2, 5, and 30 min) for (a) nano-twin Cu particles and (b) regular Cu particles. The absorption bands at 1650-1750, 1580 ± 10, 1273, 1194, 1107, and 1052 cm⁻¹, according to previous reports [62,63], are ascribed to the ν (C=O), ν (C=C), η^2 type adsorbed C-O, ν (C-C) of methylene, monodentate and bidentate adsorbed C-O group in HCP or CPEO.

On Zn(Al)(Zr)O (without Cu) with a specific surface area of 97.2 m²/g (Table S1), furfural can barely be converted. Using FA as catalyzed substrate on Zn(Al)(Zr)O, a selectivity of 100 % to HCP is obtained with a FA conversion of 40 %, under either N₂ or H₂ atmosphere. No CPEO, CPO, or CPL is detected. That means, it is the metallic Cu that is responsible for the hydrogenation of furfural-to-FA and HCP-to-CPO, while Zn(Al)(Zr)O for the conversion of FA to HCP. The conversion of FA to HCP involves the rearrangement of furan ring to five-membered carbon ring, which is reported as

referring to an acid-catalyzed Pinacol rearrangement [45]. According to the results from temperature programmed desorption of ammonia (NH_3 -TPD) (Fig. S9), the distribution of acidic strength and the number or density of acid sites for $\text{Cu}^0\text{-Zn(Al)(Zr)O-2}$ and $\text{Cu}^0\text{-Zn(Al)(Zr)O-10}$ are similar, well accounting for their similarity in the catalysis for FA conversion.

4. Conclusions

In summary, this work first reports an effective gradient reduction strategy to control the definite structure of Cu sites by producing defects-rich nano-twin Cu particles. This strategy just involves the reduction of Cu-containing LDHs simply with controlling the reduction gradient of Cu^{II} species under two chemical micro-environments, exhibiting two-step nucleation-growth processes. The nano-twin Cu particles efficiently promote the target activation of C-O and C=C in the conversion of furfural to CPO. The defects-rich Cu particles afford a CPO selectivity of 92 % with ~ 100% furfural conversion, 50 % higher than regular spherical Cu particles. The multi-stepped surface defect sites, originating from the planar defects, play a decisive role in promoting the CPO selectivity by facilitating the hydro-deoxygenation of C-O and hydrogenation to C=C in 4-hydroxycyclopentenone intermediate. The strategy reported here can be extended to development of surface defects-rich supported metal catalysts for a broad spectrum of green chemical processes.

Acknowledgements

Financial supports from NSFC of China (21521005, 91634120), National Key R&D Program of China (2017YFA0206804) and the Fundamental Research Funds for the Central Universities (ZY1936 and XK1802-6) are gratefully acknowledged. We also thank Jun Luo and Wei Xi (Tianjin University of Technology) for their help in the in situ HR-TEM measurement and discussion.

Reference

[1] M. B. Gawande, A. Goswami, F. X. Felpin, T. Asefa, X. Huang, R. Silva, X. Zou, R. Zboril, R.

- [2] B. Kühne, H. Vogel, R. Meusinger, S. Kunz, M. Kunz, Catal. Sci. Technol. 8 (2018) 755-767.
- [3] W. Wan, S. C. Ammal, Z. Lin, K. E. You, A. Heyden, J. G. Chen, Nat. Commun. 9 (2018) 4612.
- [4] H. Yang, Y. Chen, X. Cui, G. Wang, Y. Cen, T. Deng, W. Yan, J. Gao, S. Zhu, U. Olsbye, J. Wang, W. Fan, Angew. Chem. Int. Ed. 57 (2018) 1836-1840.
- [5] H. Liu, Z. Huang, F. Zhao, F. Cui, X. Li, C. Xia, J. Chen, Catal. Sci. Technol. 6 (2016) 668-671.
- [6] S. Kuld, M. Thorhauge, H. Falsig, C. F. Elkjaer, S. Helveg, I. Chorkendorff, J. Sehested, Science 352 (2016) 969-974.
- [7] M. Behrens, F. Studt, I. Kasatkin, S. Köhl, M. Hävecker, F. Abild-Pedersen, S. Zander, F. Girgsdies, P. Kurr, B. L. Kniep, M. Tovar, R. W. Fischer, J. K. Nørskov, R. Schlögl, Science 336 (2012) 893-897.
- [8] H. Xi, X. Hou, Y. Liu, S. Qing, Z. Gao, Angew. Chem. Int. Ed. 126 (2014) 12080-12083.
- [9] B. Eren, C. Heine, H. Bluhm, G. A. Somorjai, M. Salmeron, J. Am. Chem. Soc. 137 (2015) 11186-11190.
- [10] A. A. Gokhale, J. A. Dumesic, M. Mavrikakis, J. Am. Chem. Soc. 130 (2008) 1402-1414.
- [11] H. Yue, Y. Zhao, S. Zhao, B. Wang, X. Ma, J. Gong, Nat. Commun. 4 (2013) 2339.
- [12] F. Wang, R. Shi, Z.-Q. Liu, P.-J. Shang, X. Pang, S. Shen, Z. Feng, C. Li, W. Shen, ACS Catal. 3 (2013) 890-894.
- [13] L. Wang, W. Chen, D. Zhang, Y. Du, R. Amal, S. Qiao, J. Wu, Z. Yin, Chem. Soc. Rev. 48 (2019) 5310-5349.
- [14] R. G. Mariano, K. McKelvey, H. S. White, M. W. Kanan, Science 358 (2017) 1187-1192.
- [15] X. Feng, K. Jiang, S. Fan, M. W. Kanan, ACS Cent. Sci. 2 (2016) 169-174.
- [16] Y. Huang, Y. Chen, T. Cheng, L.-W. Wang, W. A. Goddard, ACS Energy Lett. 3 (2018) 2983-2988.
- [17] Y. Lu, B. Cao, F. Yu, J. Liu, Z. Bao, J. Gao, ChemCatChem. 6 (2014) 473-478.
- [18] R. Reske, H. Mistry, F. Behafarid, B. R. Cuenya, P. Strasser, J. Am. Chem. Soc. 136 (2014)

- [19] C. Xie, Z. Niu, D. Kim, M. Li, P. Yang, *Chem. Rev.* 120 (2020) 1184-1249.
- [20] C. Choi, T. Cheng, M. F. Espinosa, H. Fei, X. Duan, W. A. Goddard, Y. Huang, *Adv. Mater.* 31 (2019) 1805405.
- [21] S. Daryadel, A. Behroozfar, S. R. Morsali, S. Moreno, M. Baniasadi, J. Bykova, R. A. Bernal, M. Minary-Jolandan, *Nano Lett.* 18 (2018) 208-214.
- [22] R. Huang, Z. Sun, S. Chen, S. Wu, Z. Shen, X. Wu, J. Zeng, *Chem. Commun.* 53 (2017) 6922-6925.
- [23] D. G. Evans, R. C. T. Slade, *Struct. Bond.* 119 (2006) 1-87.
- [24] J. He, M. Wei, B. Li, Y. Kang, D.G. Evans, X. Duan, *Struct. Bond.* 119 (2006) 89-119.
- [25] P. J. Sideris, U. G. Nielsen, Z. Gan, C. P. Grey, *Science* 321 (2008) 113-117.
- [26] G. Fan, F. Li, D. G. Evans, X. Duan, *Chem. Soc. Rev.* 43 (2014) 7040-7066.
- [27] K. Yan, Y. Liu, Y. Lu, J. Chai, L. Sun, *Catal. Sci. Technol.* 7 (2017) 1622-1645.
- [28] M. Xu, M. Wei, *Adv. Funct. Mater.* 28 (2018) 1802943.
- [29] Q. Wang, J. Feng, L. Zheng, B. Wang, R. Bi, Y. He, H. Liu, D. Li, *ACS Catal.* 10 (2020) 1353-1365.
- [30] X. Meng, Y. Yang, L. Chen, M. Xu, X. Zhang, M. Wei, *ACS Catal.* 9 (2019) 4226-4235.
- [31] Q. Fan, X. Li, Z. Yang, J. Han, S. Xu, F. Zhang, *Chem. Mater.* 68 (2016) 6296-6304.
- [32] G. W. Huber, S. Iborra, A. Corma, *Chem. Rev.* 106 (2006) 4044-4098.
- [33] Li, X. Zhao, A. Wang, G. W. Huber, T. Zhang, *Chem. Rev.* 115 (2015) 11559-11624.
- [34] Z. Zhang, J. Song, B. Han, *Chem. Rev.* 117 (2017) 6834-6880.
- [35] R. Mariscal, P. Maireles-Torres, M. Ojeda, I. Sádaba, M. L. Granados, *Energy Environ. Sci.* 9 (2016) 1144-1189.
- [36] L. T. Mika, E. Csefalvay, A. Nemeth, *Chem. Rev.* 118 (2018) 505-613.
- [37] S. Chen, R. Wojcieszak, F. Dumeignil, E. Marceau, S. Royer, *Chem. Rev.* 118 (2018) 11023-11117.

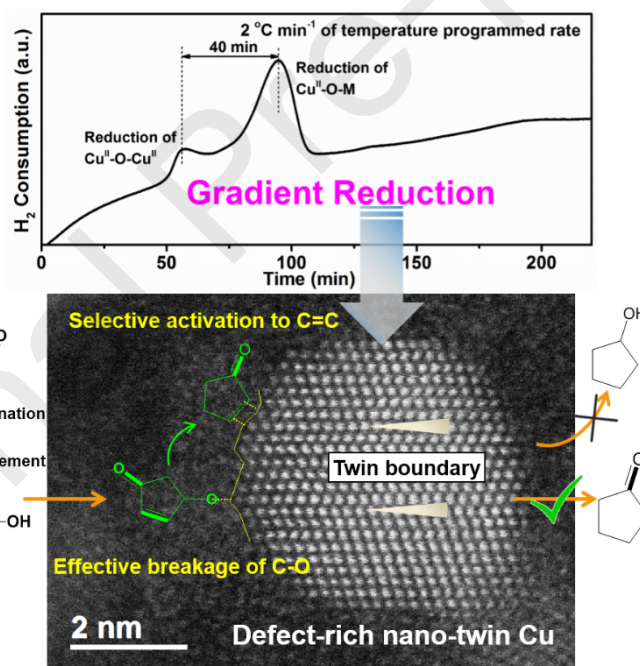
- [38] X. H. Chauderon, D. J. Chauderon, J. E. Mathiesen, Y. Qiu, J. M. Carraner, J. P. Tessonnier, W. Li, *J. Am. Chem. Soc.* 139 (2017) 14120-14128.
- [39] Y. Ma, G. Xu, H. Wang, Y. Wang, Y. Zhang, Y. Fu, *ACS Catal.* 8 (2018) 1268-1277.
- [40] Tong, X. Liu, Y. Guo, M. N. Banis, Y. Hu, Y. Wang, *J. Catal.* 365 (2018) 420-428.
- [41] R. Ma, X.-P. Wu, T. Tong, Z.-J. Shao, Y. Wang, X. Liu, Q. Xia, X.-Q. Gong, *ACS Catal.* 7 (2017) 333-337.
- [42] Y. Deng, R. Gao, L. Lin, T. Liu, X.-D. Wen, S. Wang, D. Ma, *J. Am. Chem. Soc.* 140 (2018) 14481-14489.
- [43] D. Kalaitzakis, M. Triantafyllakis, I. Alexopoulou, M. Sofiadis, G. Vassilikogiannakis, *Angew. Chem. Int. Ed.* 53 (2014) 13201-13205.
- [44] M. Hronec, K. Fulajtarová, *Catal. Commun.* 24 (2012) 100-104.
- [45] J. Scognamiglio, L. Jones, C. S. Letizia, A. M. Api, *Food Chem. Toxicol.* 50 (2012) 608-612.
- [46] M. Alas, M. Crochemore, *Eur. Patent*, 626364A1, 1994.
- [47] M. Renz, *Eur. J. Org. Chem.* 6 (2005) 979-988.
- [48] J. Guo, G. Xu, Z. Han, Y. Zhang, Y. Fu, Q. Guo, *ACS Sustainable Chem. Eng.* 2 (2014) 2259-2266.
- [49] G. W. Huber, R. D. Cortright, J. A. Dumesic, *Angew. Chem. Int. Ed.* 43 (2004) 1549-1551.
- [50] G. W. Huber, J. N. Chheda, C. J. Barrett, J. A. Dumesic, *Science* 308 (2005) 1446-1450.
- [51] M. Besson, P. Gallezot, C. Pinel, *Chem. Rev.* 114 (2014) 1827-1870.
- [52] K. Ma, Y. Tian, Z.-J. Zhao, Q. Cheng, T. Ding, J. Zhang, L. Zheng, Z. Jiang, T. Abe, N. Tsubaki, J. Gong, X. Li, *Chem. Sci.* 10 (2019) 2578-2584.
- [53] G. Pacchioni, H.-J. Freund, *Chem. Soc. Rev.* 47 (2018) 8474-8502.
- [54] C. J. G. Van Der Grift, A. F. H. Wielers, B. P. J. Jogh, J. Van Beunum, M. De Boer, M. Versluijs-Helder, J. W. Geus, *J. Catal.* 131 (1991) 178-189.
- [55] A. Gervasini, S. Bennici, *Appl. Catal. A* 281 (2005) 199-205.
- [56] W. Li, G. Fan, L. Yang, F. Li, *Catal. Sci. Technol.* 6 (2016) 2337-2348.

- [57] Y. Zhang, G. Fan, L. Yang, F. Li, *Appl. Catal., A* 361 (2018) 117-126.
- [58] P. Hollins, *Surf. Sci. Rep.* 16 (1992) 51-94.
- [59] W. Tong, A. West, K. Cheung, K.-M. Yu, S. C. E. Tsang, *ACS Catal.* 3 (2013) 1231-1244.
- [60] W. Li, Y. Li, G. Fan, L. Yang, F. Li, *ACS Sustainable Chem. Eng.* 5 (2017) 2282-2291.
- [61] Y. Tang, Y. Liu, P. Zhu, Q. Xue, L. Chen, Y. Lu, *AIChE J.* 55 (2009) 1217-1228.
- [62] J. V. Ochoa, C. Trevisanut, J.-M. M. Millet, G. Busca, F. Cavani, *J. Phys. Chem. C* 117 (2013) 23908-23918.
- [63] Z. D. Young, S. Hanspal, R. J. Davis, *ACS Catal.* 6 (2016) 3193-3202.

A Gradient Reduction Strategy to Produce Defects-Rich Nano-Twin Cu Particles for Targeting Activation of Carbon-Carbon or Carbon-Oxygen in Furfural Conversion

Yanru Zhu, Jian Zhang, Xiaodan Ma, Zhe An, Shaowei Guo, Xin Shu, Hongyan Song, Xu Xiang,
and Jing He*

An effective and convenient “Gradient Reduction” strategy is originally proposed to produce defects-rich nano-twin Cu^0 particles from Cu^{II} -containing LDHs. Based on a unique perspective onto the bonding feature in brucite-like layer of LDHs, kinetically segregated reduction of $\text{Cu}^{\text{II}}\text{-O-Cu}^{\text{II}}$ from that of $\text{Cu}^{\text{II}}\text{-O-M}$ has been revealed. The decisive role of defect Cu sites in the selective activation of target bonds in furfural-to-cyclopentanone reaction is demonstrated.



- > An effective and convenient gradient reduction strategy to construct surface defects by producing nano-twin Cu particles is presented.
- > Utilizing the bonding feature and chemical micro-environments in brucite-like layer of LDHs, a kinetically segregated reduction of $\text{Cu}^{\text{II}}\text{-O-Cu}^{\text{II}}$ from that of $\text{Cu}^{\text{II}}\text{-O-M}$ is revealed.
- > The particles efficiently promote the target activation of C-O and C=C in the conversion of furfural to cyclopentanone.
- > The defect sites on nano-twin Cu play a decisive role in promoting the cyclopentanone selectivity.

A Gradient Reduction Strategy to Produce Defects-Rich Nano-Iwin Cu Particles for Targeting Activation of Carbon-Carbon or Carbon-Oxygen in Furfural Conversion

Yanru Zhu, Jian Zhang, Xiaodan Ma, Zhe An, Shaowei Guo, Xin Shu, Hongyan Song, Xu Xiang, and Jing He*

The authors declare no competing financial interest.

Journal Pre-proofs